ACS MEASUREMENT SCIENCE Au
AN OPEN ACCESS JOURNAL OF THE AMERICAN CHEMICAL SOCIETY

pubs.acs.org/measureau

Article

Use of Magnetic Modulation of Nitrogen-Vacancy Center Fluorescence in Nanodiamonds for Quantitative Analysis of Nanoparticles in Organisms

Zachary R. Jones, Nicholas J. Niemuth, Yongqian Zhang, Connor R. Protter, Paige C. Kinsley, Rebecca D. Klaper, and Robert J. Hamers*

Cite This: *ACS Meas. Sci. Au* 2022, 2, 351−360

Read Online

ACCESS | Metrics & More | Article Recommendations | Supporting Information

ABSTRACT: The fluorescence intensity emitted by nitrogen-vacancy (NV) centers in diamond nanoparticles can be readily modulated by the application of a magnetic field using a small electromagnet. By acquiring interleaved images acquired in the presence and absence of the magnetic field and performing digital subtraction, the fluorescence intensity of the NV nanodiamond can be isolated from scattering and autofluorescence even when these backgrounds are changing monotonically during the experiments. This approach has the potential to enable the robust identification of nanodiamonds in organisms and other complex environments. Yet, the practical application of magnetic modulation imaging to realistic systems requires the use of quantitative analysis methods based on signal-to-noise considerations. Here, we describe the use of magnetic modulation to analyze the uptake of diamond nanoparticles from an aqueous environment into *Caenorhabditis elegans*, used here as a model system for identification and quantification of nanodiamonds in complex matrices. Based on the observed signal-to-noise ratio of sets of digitally subtracted images, we show that nanodiamonds can be identified on an individual pixel basis with a >99.95% confidence. To determine whether surface functionalization of the nanodiamond significantly impacted uptake, we used this approach to analyze the presence of nanodiamonds in *C. elegans* that had been exposed to these functionalized nanodiamonds in the water column, with uptake likely occurring by ingestion. In each case, the images show a significant nanoparticle uptake. However, differences in uptake between the three ligands were not outside of the experimental error, indicating that additional factors beyond the surface charge are important factors controlling uptake. Analysis of the number of pixels above the threshold in individual *C. elegans* organisms revealed distributions that deviate significantly from a Poisson distribution, suggesting that uptake of nanoparticles may not be a statistically independent event. The results presented here demonstrate that magnetic modulation combined with quantitative analysis of the resulting images can be used to robustly characterize nanoparticle uptake into organisms.

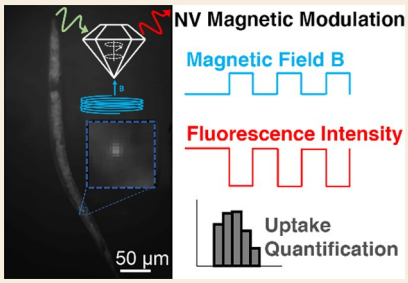

KEYWORDS: *nanodiamond, NV centers, magnetic modulation, fluorescence microscopy, C. elegans, nanoparticles*

INTRODUCTION

The growing use of engineered nanomaterials in consumer products and the potential for their unintentional release into environmental systems drive an increasing need to understand the potential impacts of nanomaterials on complex and dynamic biological systems.[1−6] To understand the overall environmental impact of nanoparticles, it is necessary to identify and understand the underlying mechanisms of biological response. While some interactions are likely to be specific to particular nanoparticle compositions,[4,7] recent data suggest that some interactions of nanoparticles can be associated with molecular properties.[8−10] For example, the surface chemistry of nanomaterials, specifically the surface charge and hydrophilicity of ligands attached to a nanoparticle, are factors that may impact the outcomes of nanomaterials by governing the formation of coronas or interactions with membranes and interfaces.[8,11−14] Identifying the impact of surface charge and other nanoparticle properties on biological systems is a complex challenge that requires highly stable nanoparticles and associated surface functionalization, along with analytical tools able to investigate their locations and interactions within organisms.[4,15]

Identification of the locations and quantities of nanoparticles within organisms by optical microscopy techniques is complicated by factors such as instability of the surface ligands, bleaching of the fluorescence probes, and the complex optical properties (e.g., spatially varying index of refraction, scattering, and absorption) of multicellular organisms.[16−19] Recently, diamond nanoparticles have emerged as a system of

Received: February 3, 2022
Revised: April 6, 2022
Accepted: April 20, 2022
Published: May 12, 2022

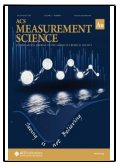

ACS Publications

© 2022 The Authors. Published by American Chemical Society

https://doi.org/10.1021/acsmeasuresciau.2c00006
ACS Meas. Sci. Au 2022, 2, 351−360

interest because diamonds can be covalently functionalized with molecular layers with unparalleled chemical stability[8,14,17,20,21] while also being able to host stable fluorescent defects such as nitrogen-vacancy (NV) centers that enable unique imaging capabilities.[22−24] Consequently, diamond nanoparticles can overcome many of the limitations of fluorescence microscopy through superlative properties of photostability, red emission, biocompatibility, and spin-dependent luminescence properties.[16,18,25−28] One unusual property of NV centers is that they have unpaired spins with very long coherence times, such that their fluorescence properties depend on the spin-state of their electrons. As a result, the application of modest magnetic fields on the order of a few Gauss can modulate the fluorescence intensity by up to 20%.[29−31] This high sensitivity to magnetic fields can be used to distinguish the nanodiamond from other sources of light emission, such as scattering and autofluorescence.[29,30,32,33] The ability to modulate NV-center fluorescence has enabled detection and imaging in a variety of cellular and cell-model systems and imaging in a few organismal systems.[32−35] These modulation-based imaging techniques provide a valuable supplement or alternative to other methods used to image in high fluorescence backgrounds. In contrast to methods like fluorescence lifetime imaging or two-photon excited fluorescence that require specialized pulsed excitation or time-gated detection,[36−38] magnet-induced modulation can be incorporated into existing confocal or wide-field microscopes using an inexpensive electromagnet and a simple current source. The high (50%) duty cycle further yields good counting statistics using low-powered illumination sources beyond proof-of-principle; however, identification and quantification of the NV-nanodiamond are complex endeavors with challenges that are specific to the system of study. Organism-to-organism heterogeneity, fluctuations in autofluorescence, and light absorption considerations related to tissue penetration can complicate the detection and create the need for a robust process for collecting and analyzing images to confidently identify the presence of a nanodiamond above the background.

In this study, we investigate how to optimize magnetically modulated image collection and analysis as a foundation for the quantitative study of nanodiamond uptake within organisms. We use the aquatic organism *Caenorhabditis elegans* (*C. elegans*) as a model system due to its wide use and merit as a model organism in many fields of science.[39] We perform magnetic modulation of the NV center intensity from diamond nanoparticles ingested by the organisms to identify how different experimental measurement conditions and image analysis processes affect the ability to robustly identify nanodiamonds within this organism. We especially focus here on a statistical analysis of the magnetically modulated images and how to robustly extract information from the images. Building upon previously published procedures to functionalize nanodiamonds with varying surface ligands,[20] we compare the effects of the surface charge and ligand length on NV-containing nanodiamond (NVND) uptake within the *C. elegans*. We also discuss some of the limitations of these methods in organisms, including attenuation of excitation intensity by the biological tissue. Ultimately these studies provide insights into the practical implementation of magnetically modulated imaging to selectively identify nanodiamonds within complex systems.

METHODS

Optical Measurements

All fluorescence measurements were performed on a custom-built microscope system that has been described previously.[29] Briefly, a 532 nm laser excitation from a diode laser (Opto Engine LLC-500 mW) is stabilized to an output of 400 mW using a beam stabilizer (Brockton BEOC-LPC) and then directed through a 2× beam expander (Thorlabs), through a 532 nm (22 nm bandwidth) bandpass filter (Semrock FF02-531/22-25) and a dichroic mirror (Semrock, FF-596-Di01-22 × 36 or Semrock, FF-552-di02 for spectroscopy). The incident light is reflected toward a microscope objective turret that has a 20× objective (Nikon PlanFluor, 20× 0.5 NA) and a 40× objective (Nikon PlanFluor, 40× 0.75 NA). The red emission collected by the objective passes through the dichroic mirror and a 532 nm line reject filter (Semrock NF01-532U-25) to a tube lens (Thorlabs TTL-200A) that forms a real image. The image is transferred using a 4f correlator either to the imaging camera (Andor IXON Ultra 888), to a spectrograph (Andor Shamrock 193i) with an attached CCD (Andor iStar) for fluorescence spectra, or to an avalanche photodiode for photon counting (Excelitas SPCM-AQRH-14). The filter configuration was chosen in order to maximize the NV center emission collected in our images.

Magnetic modulation fluorescence images were collected using a 20× objective and the imaging EMCCD. Applied magnetic fields come from a small electromagnet (Uxcell, 12 V 50 N) placed about 2 mm from the sample surface and powered using a sourcemeter (Keithley 2425 100 W), which applies a constant current of 0.35 A for magnet on or 0 A for magnet off. Imaging conditions during exploratory experiments were optimized to maximize photon counts while minimizing imaging time. Images collected to compare functionalization effects were made by accumulating 10 imaging cycles. Each cycle consisted of a 0.25 s exposure accumulated 20 times with the magnet on and then a 0.25 s exposure accumulated 20 times with the magnet off. We used a constant gain setting of 30. Magnet on/magnet off cycles were repeated 10 times. Integration time plus programing delays resulted in total imaging time of approximately 2.5 min. Fluorescence spectra and modulation comparisons were measured using the 40× objective sent to the spectrometer or to the avalanche photodiode, with magnetic fields applied in the same manner.

Experiments were controlled using a custom-written LabView program that initializes the EMCCD, applies current to the electromagnet, and begins image collection. Data were obtained using a sequence of individual image acquisition, alternating between acquisitions with the magnet on and those with the magnet off. Image processing, including loading image files, mathematical operations on images, thresholding, and statistics, was performed using Igor Pro (WaveMetrics), except for time-dependent intensity plots, which were generated using FIJI (ImageJ).[40]

Fluorescence spectra of functionalized diamonds were collected by drying a drop from suspension onto a coverslip and measured using a monochromator (Andor Shamrock) with an attached intensified CCD (Andor iStar). Spectra were collected on a grating with 300 lines/mm blazed at 300 nm and normalized to their maximum point. Each ligand type was measured at 3 locations, and their spectra were averaged.

Nanoparticle Functionalization

All chemicals were purchased from Sigma-Aldrich unless otherwise specified. NVND used in these studies was purchased from Adamas Nanotechnologies, with an average diameter of 40 nm. These diamonds are made from diamonds synthesized by high-pressure, high-temperature methods, followed by NV center activation and finally conversion to nanometer sizes via mechanical methods. The resulting nanoparticles can be seen in the scanning electron micrographs in Figure S1 and are irregular in shape, with multiple exposure facets. Nanopure water was purified to 18 MΩ cm using a Barnstead GenPure system.

https://doi.org/10.1021/acsmeasuresciau.2c00006
ACS Meas. Sci. Au 2022, 2, 351−360

Ligand synthesis and functionalization procedures have been reported previously[14,20] and are briefly summarized below. The nanodiamond was first hydrogen-terminated by heating in a tube furnace at 750 °C for 5 h under an atmosphere of H_2 at atmospheric pressure; we used a typical sample size of 10 mg of NVND. After cooling overnight, the nanoparticles were transferred into a glovebox for surface functionalization. The functionalization procedure here was reported previously and consists of using a radical initiator (benzoyl peroxide) to activate surface sites on the nanodiamond sample, which then react with the terminal alkenyl group of the desired reactant molecules. In a nitrogen atmosphere glovebox, 10 mg of benzoyl peroxide in 1 mL benzene was combined with either 140 mg of allyl trimethylammonium bromide (yielding C3 quaternary amine-terminated particles), 140 mg of 11-trimethylammonium-1-undecene (yielding C11 quaternary amine-terminated particles), or 40 μL of 4-pentenoic acid (yielding COOH-terminated particles), before drying over molecular sieves. Each reaction mixture was added to a vial containing NVND, sealed, and stirred at 80 °C for 3.5 h in an oil bath, and allowed to cool overnight.

After cooling, each solution was resuspended in 15 mL of benzene, sonicated, and centrifuged at 4700*g* for 15 min. This was repeated twice more in acetone, and three times in Nanopure water, to ensure particles were cleaned prior to further studies. Finally, each set of particles was resuspended in 2.5 mL of Nanopure water. Some particle batches remained somewhat polydisperse after washing steps and were allowed to settle overnight before separating the supernatant from the settled pellet. In these cases, the supernatant was used.

We measured the hydrodynamic diameter using dynamic light scattering (DLS) and measured the zeta potential using electrophoretic mobility measurements, both performed on a Malvern Zetasizer. These measurements were performed in Nanopure water.

Nanoparticle concentrations were measured gravimetrically by weighing a known amount of nanodiamond dried from suspension using a microbalance (Sartorius MSE6.6s). Concentration measurements were performed in triplicate and averaged.

C. Elegans Culture and Exposure

Wild-type N2 *C. elegans* and OP50 *Escherichia coli* were obtained from the Caenorhabditis Genetics Center (University of Minnesota, Minneapolis, MN). *C. elegans* were cultured on OP50-seeded solid nematode growth medium (NGM) plates at 20 °C following standard protocols.[41]

Exposure solutions consisted of 500 μL of C3, C11, or PA NVND suspended in water at 300 μg/mL (500 μL sterile water for controls), which were each added to 500 μL of the concentrated OP50 bacteria. Each solution was then vortexed to yield final NVND exposure concentrations of 150 μg/mL. Exposure plates consisted of 1 mL of each exposure solution added to a 100 mm NGM plate in triplicate, dried overnight in a fume hood.

Synchronized L1 larvae were obtained by bleaching gravid adults to obtain eggs.[41] These eggs were then placed on an unseeded NGM plate overnight to synchronize hatched larvae at the L1 stage. For exposures, synchronized L1 larvae were washed from this NGM plate using sterile M9 media, pelleted at 2500*g* 20 °C for 1 min, and resuspended in M9 at 10 larvae per μL. 100 μL of this solution, or approximately 1000 larvae, were then added to each exposure plate. Three replicates were exposed to C3, C11, or PA NVND or a water control for 48 h.

C. Elegans Fixation for Imaging

After 48 h total, larvae were washed from exposure plates with sterile M9, pelleted at 2500*g* for 1 min, washed 3 times with sterile M9, and fixed in 4% paraformaldehyde for 10 min. Fixed larvae were then pelleted at 2500*g* for 1 min, rinsed 3 times with 1× phosphate-buffered saline, and stored at 4 °C for further analysis.

Fixed *C. elegans* were imaged by dropping 10 μL of the suspension containing the organisms along with 10 μL of Nanopure water onto a coverslip. The wet organisms were sealed between 2 coverslips using clear nail polish; this procedure allow the organisms to remain in aqueous medium while minimizing drying and fluid motion.

RESULTS AND DISCUSSION

NV centers in the negative charge state contain two unpaired electrons that result in the formation of a spin-triplet in the ground state of the NV center.[25] Differences in the rates of relaxation between the possible pathways result in a more intense emission from the $m_s = 0$ spin state compared to the $m_s = \pm 1$ states. The dimmer $m_s = \pm 1$ states are degenerate and separated from the $m_s = 0$ state by an energy gap corresponding to a frequency of 2.87 GHz in the absence of a magnetic field, and the relative populations of these states are sensitive to external factors like resonant microwaves, spin-noise, and magnetic fields. We make use of these properties by measuring the fluorescence of NV-nanodiamond (NVND) in the presence and absence of a modest magnetic field.

Nanodiamond Functionalization

To study the effects of diamond surface functionalization on the uptake and location within *C. elegans*, we selected three ligand types. Figure 1a shows the structures of the ligands,

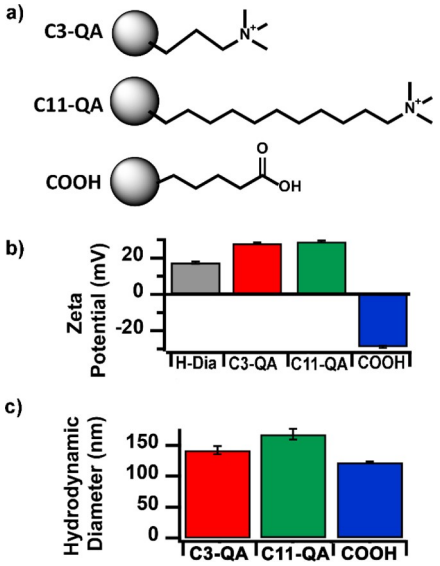

Figure 1. (a) Schematic of the structures of NVND functionalized with the three ligands described here. (b) Zeta potentials for the H-terminated nanodiamond (H-Dia) and functionalized nanodiamond (c) hydrodynamic diameters. Error bars represent standard deviations from 3 (zeta potential) or 5 (diameter) replicate samples.

which include a quaternary amine headgroup attached to a three-carbon linker (C3-QA), a quaternary amine attached to an eleven-carbon linker (C11-QA), and a pentanoic acid ligand (COOH). These three ligand types were chosen to represent a range both in charge, with the quaternary amine headgroups imparting positive charges, and in ligand length, which have both been shown to affect nanoparticle outcomes in organisms.[9,11,14,42,43]

In previous studies, we established the ability to functionalize nanodiamonds with these three ligands and characterized their surface charge and other relevant properties.[14,20,43] Here, we further verified successful functionalization using zeta potential measurements, which are an indication of the surface charge of a nanoparticle in the solution. Figure 1b shows zeta potentials for H-Dia and the functionalized samples. While the as-received nanodiamond has a negative zeta potential due to surface carboxylate groups (Figure S2),[44] Figure 1b shows that

https://doi.org/10.1021/acsmeasuresciau.2c00006
ACS Meas. Sci. Au 2022, 2, 351−360

after hydrogen termination, the nanodiamond has a positive zeta potential of +17 mV. Grafting of long-chain (C11) and short-chain (C3) quaternary amine-functionalized NVND increases the zeta potential to approximately +29 mV. This increase in the magnitude of the zeta potential indicates the presence of more positive charges at the surface, consistent with the addition of the charged C11-QA and C3-QA ligands. In contrast, Figure 1b shows that grafting with pentanoic acid to produce COOH-functionalized NVND yields a zeta potential of −29 mV; the shift back to a strongly negative potential is consistent with the presence of deprotonated carboxylic acid groups terminating this ligand.

To ensure comparisons of the ligand identity are not affected by drastic size changes, we also measured the hydrodynamic diameter of the functionalized nanodiamond. Figure 1c compares the sizes of each functionalized NVND population. The as-received diamond has a 40 nm core, as confirmed by scanning electron micrographs and DLS measurements shown in Figures S1 and S2. After functionalization, all ligand types show a hydrodynamic diameter that is larger than the combination of the core size and the expected length of the ligands attached, indicating that some aggregation occurs during functionalization or washing. While the nanoparticles aggregated, the sizes of the functionalized nanodiamond to be compared were similar, ranging between 120−170 nm. The DLS and zeta potential measurements show that we successfully prepared NVND with comparable sizes and with either positive or negative charges.

Optical Properties of the Functionalized NVND

To ensure that optical measurements are not significantly affected by the diamond surface chemistry, we measured the fluorescence properties of the functionalized NVND. The presence of charges near the NVND surface could potentially impact the quantum properties of the NV centers within either by causing charge-state changes[45−48] or by causing a decrease in the lifetime of the spin-polarized state.[31] To identify any potential effect of surface functionalization on the NV center charge state, we measured fluorescence spectra of the functionalized NV nanodiamond. Figure 2a shows the spectra of each type of functionalized diamond normalized to the maximum in each spectrum. The fluorescence emission begins at 575 nm and extends to about 800 nm, which indicates the presence of NV centers in neutral (NV^0) and negative (NV^-) change states. The emission from NV centers consists of contributions from the neutral NV^0 charge state starting at 575 nm and extending to approximately 700 nm, and contributions from the negative NV^- charge state, which starts at 637 nm and extends to about 800 nm.[25,49] Each measurement, which incorporated several nanodiamonds in a field of view, displayed small variations in the NV^0 versus NV^- content, but all samples are comparable in the ratio of charge states present. These spectra imply that NVNDs with a 40 nm NVND core contain enough NV centers per particle to ensure that even if one or a few NV centers are near enough to the surface to be affected by the ligands attached, these changes happen in the context of many NV centers, limiting their effect on the overall fluorescence of the nanodiamond.

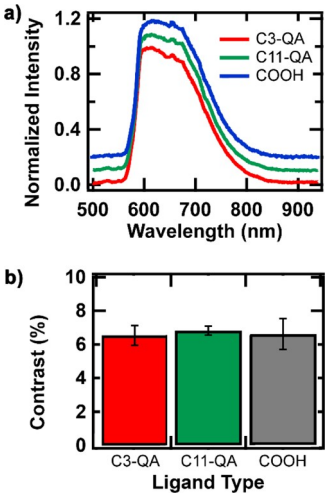

Figure 2. Fluorescence spectra of functionalized NVND. NV^0 charge state emits from 575 to 700 nm while NV^- charge state emits 638−800 nm. (B) Magnet on−off contrast measured as an ensemble. Error bars represent the standard deviation of 3 measurements.

To further identify whether the surface functionalization impacted the overall spectroscopic properties of the NVND, we measured the response of NV^- centers in each sample to an applied magnetic field. If the attached molecules impact the spin lifetimes of the NV center electrons, the amount that the fluorescence modulates in a magnetic field may decrease. Figure 2b shows the percent change in fluorescence intensity longer than 700 nm (from NV^- centers only) in each sample type under applied magnetic field relative to the zero-field emission. All three sample types modulate nearly 6% in response to the magnetic field. The absolute value of this contrast is dependent on many factors including the illumination intensity and applied magnetic field strength,[29] but under the same conditions, a difference in the contrast would indicate material property differences that may complicate imaging experiments. The consistency of the emission spectra and response to the magnetic field indicates that NVND functionalization does not significantly impact NV center fluorescence or quantum properties.

Fluorescence Images of *C. Elegans*

Figure 3a shows a representative fluorescence image of fixed *C. elegans* that were not exposed to the fluorescent nanodiamond. The image shows that the fixed organism emits a significant amount of autofluorescence that enables the identification of the location of the organism itself and the structures and tissue within. The images in Figure 3 were collected by accumulating 20 exposures of each image under an applied magnetic field followed by the same collection in the absence of a magnetic field, then repeating this on−off cycle 10 times for a total of 20 image frames. Figure 3a shows only the first frame of this image cycle, with the magnetic field applied. A representative image of NVND-exposed *C. elegans* collected in the same manner and displaying the first image frame is shown in Figure 3b. This image displays a similar situation to the nonexposed organism, in which the organism emits bright autofluorescence throughout. In the exposed case, however, several small areas of a brighter emission can be observed, as highlighted in the inset of Figure 3b.

Over the duration of this image sequence, the autofluorescence in the *C. elegans* photobleaches, decreasing the number of measured fluorescence counts over time. Figure 3c shows the average intensity in each image frame, both for a region of the nonexposed organism designated in the image by the grey dashed lines (black trace, square markers) and for a region of

https://doi.org/10.1021/acsmeasuresciau.2c00006
ACS Meas. Sci. Au 2022, 2, 351−360

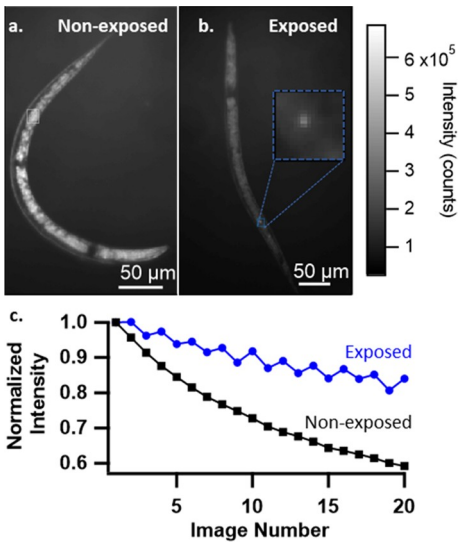

Figure 3. (a) Fluorescence images of a representative *C. elegans* that was not exposed to NVND; (b) fluorescence image of *C. elegans* that was exposed to NVND, with inset showing a localized region of a higher fluorescence intensity. (c) Intensity change with time in the region denoted by the white dotted line in panel (a) and the region denoted by the blue dotted lines in panel (b).

the exposed organism designated by the blue dashed lines (blue trace, round markers). The black trace showing the region in the control worm demonstrates that this autofluorescence decreases by about 60% from the first image to the 20th image. The blue trace shows the change in fluorescence over time of one of the small bright areas in the organism, demonstrating a smaller decrease in intensity and a noticeable response to the magnetic field. The emission in this trace decreases slightly (around 10−15%) over the 20 image frames and fluctuates during each frame, increasing by a few percent in the absence of the magnetic field as compared to the presence of a magnetic field. The smaller magnitude of the decreasing signal over the imaging time in combination with the ostensible response to the magnetic field indicates that the small bright spots in the images of exposed *C. elegans* are likely from the NV nanodiamond, while the more diffuse emission throughout the rest of the organism and in the controls is likely autofluorescence.

Magnetic Modulation for Background Removal

We have developed a general protocol for imaging and analyzing the locations and quantities of the NV nanodiamond within the *C. elegans*. The process, each step of which is discussed in more detail below, consists of four main steps: (1) collect fluorescence images in the presence and absence of a magnetic field at all wavelengths from 550 nm to the wavelength limit of the CCD (about 900 nm); (2) subtract the "magnet-on" images from the "magnet-off" images. Because of a steadily decreasing signal that results from organism autofluorescence photobleaching over time, a direct subtraction results in a negative background for organism autofluorescence. This is accounted for by using a "central difference" subtraction and averaging, taking the average of the 2 "on" images before and after each off image to create 1 difference image, then averaging the results over repeated cycles to yield a final "difference image;" (3) normalize the difference image to the average of the "magnet-off" images to show the percentage change in response to the applied magnetic field ("percent contrast" image); (4) apply a threshold to the percent contrast image to isolate the locations of NV nanodiamonds.

Figure 4 summarizes the results of using this protocol. Figure 4a shows representative fluorescence images of *C. elegans* that were exposed to C11-QA-NVND (long chain, positively charged ligand) as the average of all the "magnet-off" images collected. The organism itself can be located by its autofluorescence which displays the outline of the organism and, in some cases, reveals some internal structures. The head of this organism is in the top left of the image, and the tail curls back over the rest of the organism near the middle of the image. In addition to the autofluorescence of structures within the organism, there are several small brighter spots throughout, which are presumed to be fluorescent diamond nanoparticles and aggregates. The NVND appears to remain within the gut, a long tube-like structure running from the head to the tail of the organism, and in clusters near what is likely the grinder (a cavity in which food is ground before passing to the rest of the organism). Some apparent particles or aggregates are brighter than the autofluorescence from the organism, as is the case in the example that is traversed by the dashed line labeled "line 1". Other particles are of comparable brightness or obscured by

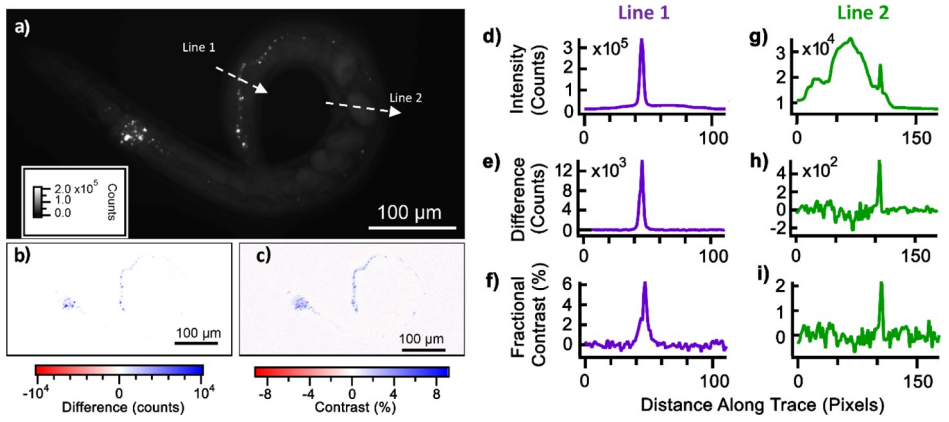

Figure 4. Images of *C. elegans* exposed to NVND. (a) Fluorescence image of *C. elegans* after exposure to NVND; (b) difference image obtained by subtracting the magnet-on image from the magnet-off image; (c) percent contrast resulting from dividing the difference image by the average of the magnet-on and magnet-off images. (d−i) Line profiles obtained from the image data along the lines indicated in panel (a).

https://doi.org/10.1021/acsmeasuresciau.2c00006
ACS Meas. Sci. Au 2022, 2, 351−360

the autofluorescence, as is the case in the example highlighted in "line 2."

Identification of the Nanodiamond

In our previous study, we demonstrated how the magnet-induced modulation of NV fluorescence helps to increase the selectivity of imaging for the nanodiamond. As noted above, the raw images of *C. elegans* show fluorescence both from the nanodiamond and autofluorescence. This can be seen more clearly by examining intensity profiles, or line scans, taken along different parts of the image. The path labeled "Line 1" in Figure 4a produces the intensity profile shown in Figure 4d, which passes through a particularly bright area that can be reasonably assumed to be an NV nanodiamond within the organism along with a weaker background that we attribute to autofluorescence. In contrast, the intensity profile in Figure 4g along the line labeled "Line 2" passes through both a bright area of autofluorescence within the organism between 0 and 100 pixels along the trace and a nanodiamond that is emitting a similar number of photons near 100 pixels along the trace. In this situation, identification of NVND is qualitatively possible but quantitatively more difficult and less certain.

By applying the magnetic modulation and image subtraction described above, the confidence with which the diamond can be identified greatly increases. We imaged the location shown in Figure 4a in the presence and the absence of a magnetic field, subtracted the results as described above, then averaged over repeated cycles ($N = 10$) to create the difference image shown in Figure 4b. The image is displayed with a color scale from red for negative values to blue for positive values, with white being zero.

The line scans shown in Figure 4e,h demonstrate the quantitative advantages of magnetic modulation for background removal in these images. The line labeled line 1, passing through the same region as shown in the fluorescence image, displaying a similar situation in the difference profile in which the NVND emission is sharp and positive. Notable in the difference trace, however, is that whereas the NVND signature in the line scan remains positive, the contribution to the signal from the organism is now effectively zero. This removal of the nondiamond background provides a way to qualitatively determine the identity of fluorophores, as those that remain positive in this imaging configuration can be reasonably assumed to be from the diamond rather than from autofluorescence.

The line scan labeled line 2, which passes through the same dimmer diamond discussed above, emphasizes the power of the magnetic modulation technique. While the emissions from the diamond and the organism were comparable in the fluorescence image, after modulation and image subtraction, the NVND difference counts are positive while the autofluorescence emission is removed. This example demonstrates the ability to locate NVND within *C. elegans* samples that have a high autofluorescence background using magnetic modulation of NV fluorescence.

While the difference image is informative in identifying and locating the nanodiamond in the context of autofluorescence, normalizing the difference image by the average intensity yields a "percent contrast" that provides a more quantitative way of distinguishing the nanodiamond from other emitters or scatterers. The "percent contrast" image shown in Figure 4c shows the NVND intensity percent change in response to the magnetic field on a pixel-by-pixel basis, shown on a color scale with positive changes in blue, negative changes in red, and zero in white. In the case shown, NV centers modulate up to 8% and are seen as blue areas in the image. The percent contrast scale also allows for a rapid evaluation of potential artifacts during automated processing of images; for example, the theoretical maximum modulation of NV centers is limited to ~30%,[26] while small negative changes outside of the limits set by Poisson counting statistics can indicate a problem with the experiment. This type of problem happens, for example, when the organism moves between adjacent frames. More generally, the percent contrast value is a more robust way to conclusively establish that features observed in the difference images arise from NVND.

Thresholding and NVND Quantification

The quantity of NVND in an organism can be quantified in two steps: (1) implementing a thresholding technique to establish whether each individual pixel in an image corresponds to the fluorescence from NVND, and (2) for those pixels whose fluorescence is attributed to NVND, using the absolute value of the fluorescence that is observed as a measure of the amount of NVND at the location of that pixel.

In order to reliably identify the amount of the diamond present in each organism, we determined a threshold based on the intensity and fractional contrast measurements using control samples of *C. elegans* that were not exposed to NVND but were otherwise prepared and measured identically to the NVND-exposed organisms described above. We established a region-of-interest (ROI) around the border of each organism and extracted the average and standard deviation of the pixels in the ROI. The average values of intensity within each organism were nearly zero, ranging from −0.4% at the most extreme to 0.02%, demonstrating that the image subtraction and normalization are highly effective at rejecting autofluorescence and scattering from non-NVND sources. By repeating this analysis using many control organisms, a global threshold can be identified that represents the upper limit of the percent contrast that can be expected from the organism's background. While, in principle, statistical limits could be identified purely on the basis of Poisson counting statistics, using experimental control samples in the manner described above is more robust as it directly accounts for additional factors such as "hot pixels" and other non-Poisson sources of noise. Once the threshold is established, a simple image mask can be applied to determine (1) how many pixels exceed the threshold, and (2) what is the total fluorescence intensity from these pixels. The latter quantity is a measure of the amount of NVND that was taken up and remaining in the organisms at the time of fixation.

Figure 5 shows the influence of the above processing steps on a typical data set. Figure 5a shows a conventional fluorescence image (i.e., without magnetic modulation) of a *C elegans* that was exposed to NVND nanoparticles that were functionalized with the C11-QA ligand. Figure 5b is an enlargement of the region indicated by the dashed lines. The conventional fluorescence images in Figure 5a,b show that this organism exhibits very little apparent NVND emission in comparison with the autofluorescence and scattering. Magnetic modulation and normalization, as described above, yields the percent contrast image in Figure 5c, showing the percent change of fluorescence in response to the applied magnetic field on a pixel-by-pixel basis. This percent contrast image shows three regions that appear to have modulation between 1

https://doi.org/10.1021/acsmeasuresciau.2c00006
ACS Meas. Sci. Au 2022, 2, 351−360

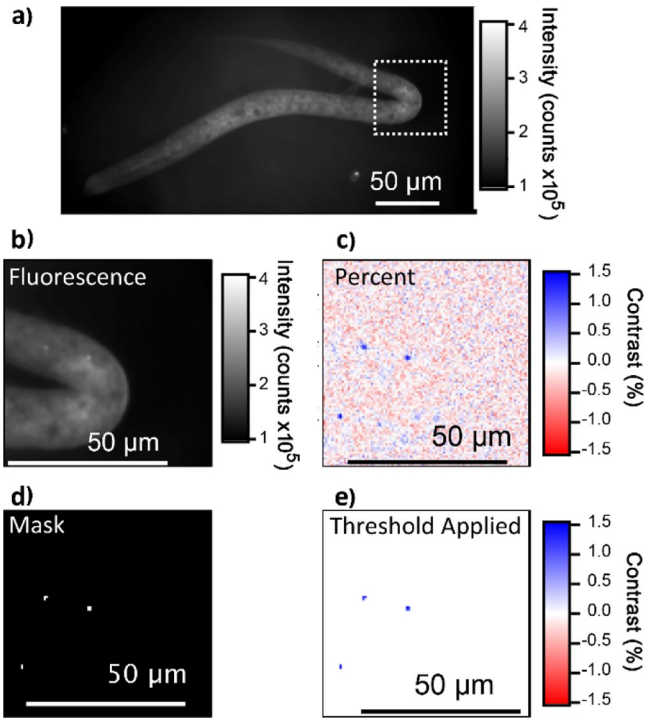

Figure 5. Fluorescence images and magnetically induced contrast from a *C. elegans* that was exposed to NVND. (a) Fluorescence image of whole *C. elegans*; the dotted region represents the region used for the subsequent analysis in frames (b–d). (b) Fluorescence image; (c) magnetically induced contrast of the same expanded region. (d) Threshold mask indicating pixels above threshold; (e) result of applying the threshold mask to the percent contrast image, leaving only NVND.

and 1.5%, while the rest of the image shows only smaller fluctuations near zero, appearing as a red and blue speckle. Notably, the outline of the organism is not detectable in the percent contrast image, demonstrating an effective removal of the autofluorescence. Measurements using control samples of nonexposed organisms yielded a standard deviation in a fractional contrast of σ = 0.324%. We, therefore, set a value of 0.97% (3σ) as our criterion for the identification of NVND in each pixel; we anticipate that there is a 99.7% certainty that values above the threshold are associated with NVND emission. Figure 5d shows the binary image that results from applying the 0.97% threshold criterion to the percent contrast image in Figure 5c. In Figure 5d, pixels exhibiting a contrast of >0.97% are white (binary 1) and identified NVND with a >99.7% certainty. The thresholding establishes that the three regions of higher modulation are from NV center fluorescence in diamond nanoparticles, while all other emissions modulated less than the threshold and were removed.

This mask can be applied in different ways to gain information about the sample. We generated a threshold-applied percent contrast image shown in Figure 5e, which shows that all nondiamond emissions have been removed and reveals the locations of NVND with no autofluorescence background. Alternatively, applying the mask to the original fluorescence image can add to the quantification by showing the total intensity in the image that comes from NV centers, under the assumption that the local concentration of NVND is proportional to the intensity of NVND emission from the corresponding image pixel.

Influence of NVND Functionalization on Nanoparticle Uptake

As an initial demonstration, we examined the influence of nanodiamond surface functionalization on the uptake of NVND by *C. elegans*, using a model set of positively charged, negatively charged, and neutral surface ligands. For the purposes of these experiments, we define uptake to represent any diamond that is ingested and remains in the organisms at the time of fixation and imaging. Our analysis of an initial exploratory dataset using this method suggested that exposing *C. elegans* larvae to functionalized NVND yielded functionalization-dependent differences in the organism size and the amount of the nanodiamond present. We, therefore, designed experiments to measure these differences, as described in the Methods section. Briefly, we exposed populations of synchronized *C. elegans* larvae to the functionalized nanodiamond in triplicate. We used triplicate control groups to determine a threshold of 0.971% using the method described above and maintained, as much as possible, the concentration of the nanodiamond between exposure groups. Images from each exposure group indicate that the organisms are smaller in size than our initial dataset and ingested or retained fewer diamond particles.

Figure 6a shows a histogram of the number of above-threshold pixels obtained for a total of 108 images (36 images

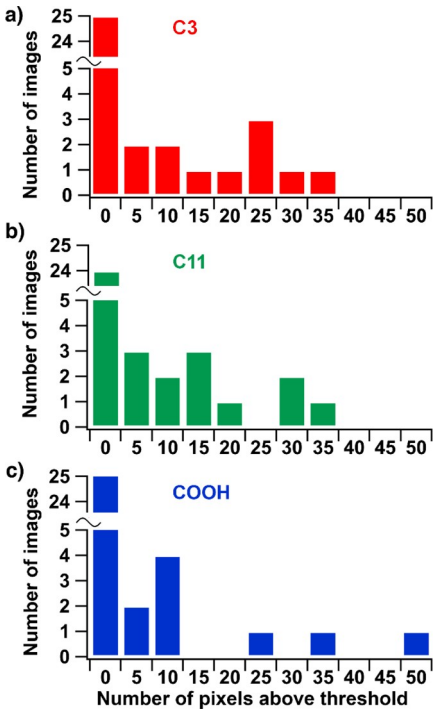

Figure 6. Histogram showing the distribution of above-threshold pixels observed from 36 samples of each of the three different functionalization chemistries used here.

for each functionalization chemistry, with each image containing a single organism). Most images contain fewer than 5 pixels above the threshold. Since nanoparticles are discrete objects, one might anticipate that the number of pixels above the threshold would follow a Poisson distribution. Attempts to fit histograms like those in Figure 6 to a Poisson distribution yield unsatisfactory results because while most images have very few (0 or 1) pixels above the threshold, some

https://doi.org/10.1021/acsmeasuresciau.2c00006
ACS Meas. Sci. Au 2022, 2, 351–360

images show a much larger number. We further analyzed the data by determining the average number of pixels above the threshold in Figure 7a and by determining the total integrated

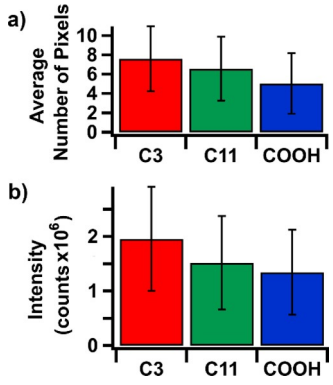

Figure 7. Results of NVND quantitative analysis in *C. elegans* exposed to the functionalized nanodiamond. (a) Average number of pixels in each organism above the threshold. (b) Average intensity above the threshold. A threshold of 0.971% modulation was used. Error bars represent 95% confidence intervals based on Gaussian statistics.

intensity of the pixels that were above the threshold (Figure 7b) by summing the raw intensity values of all pixels having a fractional modulation value that exceeded the threshold. Under the conditions of the experiments reported here, the differences in uptake between nanoparticles with different surface functionalization are not distinguishable. This, in turn, suggests that processes such as nanoparticle aggregation may be playing an important role in controlling the uptake. Previous studies comparing the biological impact of positively and negatively charged nanoparticles in other organisms[8] have reported that aggregation can be an important contributing factor. Further investigation will be required to fully ascertain the potential image of nanoparticle functionalization on uptake.

CONCLUSIONS

The ability to study the locations of nanomaterials within organisms is an important part of understanding the factors that govern nanomaterial uptake, transport, and potential toxicity. We have presented methods to reliably quantify and image the locations of nanodiamonds within the model organism *C. elegans*. The methods and analysis presented here demonstrate that magnetic modulation techniques can be used to isolate the fluorescence emitted by diamond NV centers even in complex matrices and that this can be used as a basis for more quantitative analysis of nanoparticle uptake by complex organisms. While the experiments reported here do not show significant differences in how nanoparticles with different surface functionalization are taken up into *C. elegans*, the methods implemented here are general and could be applied to quantify the nanodiamond concentration in other environments and organisms. By analyzing different collection and workup methods and determining a statistically justified threshold, we present a method for applying magnetically modulated imaging for background removal and particle identification that can add useful information to the study of nanomaterial biological interactions.

ASSOCIATED CONTENT

Supporting Information

The Supporting Information is available free of charge at https://pubs.acs.org/doi/10.1021/acsmeasuresciau.2c00006.

SEM images of the nanodiamond and DLS measurements of the nanodiamond (PDF)

AUTHOR INFORMATION

Corresponding Author

Robert J. Hamers − *Department of Chemistry, University of Wisconsin−Madison, Madison, Wisconsin 53706, United States;* orcid.org/0000-0003-3821-9625; Email: rjhamers@wisc.edu

Authors

Zachary R. Jones − *Department of Chemistry, University of Wisconsin−Madison, Madison, Wisconsin 53706, United States;* Present Address: Lawrence Berkeley Laboratory, 1 Cyclotron Road, Berkeley, California 94720, USA

Nicholas J. Niemuth − *School of Freshwater Sciences, University of Wisconsin−Milwaukee, Milwaukee, Wisconsin 53204, United States;* orcid.org/0000-0002-4463-9469

Yongqian Zhang − *Department of Chemistry, University of Wisconsin−Madison, Madison, Wisconsin 53706, United States*

Connor R. Protter − *Department of Chemistry, University of Wisconsin−Madison, Madison, Wisconsin 53706, United States;* orcid.org/0000-0003-3460-5449

Paige C. Kinsley − *Department of Chemistry, University of Wisconsin−Madison, Madison, Wisconsin 53706, United States;* orcid.org/0000-0002-0044-4782

Rebecca D. Klaper − *School of Freshwater Sciences, University of Wisconsin−Milwaukee, Milwaukee, Wisconsin 53204, United States;* orcid.org/0000-0002-9239-6916

Complete contact information is available at: https://pubs.acs.org/10.1021/acsmeasuresciau.2c00006

Author Contributions

The manuscript was written through the contributions of all authors. All authors have given approval to the final version of the manuscript.

Notes

The authors declare no competing financial interest.

ACKNOWLEDGMENTS

This study was supported by the National Science Foundation under grant no. CHE-2001611 and the NSF Center for Sustainable Nanotechnology. The CSN is a part of the Centers for Chemical Innovation Program.

REFERENCES

(1) Gantt, B.; Hoque, S.; Willis, R. D.; Fahey, K. M.; Delgado-Saborit, J. M.; Harrison, R. M.; Erdakos, G. B.; Bhave, P. V.; Zhang, K. M.; Kovalcik, K.; Pye, H. O. T. Near-road modeling and measurement of cerium-containing particles generated by nanoparticle diesel fuel additive use. *Environ. Sci. Technol.* **2014**, *48*, 10607−10613.

(2) Vance, M. E.; Kuiken, T.; Vejerano, E. P.; McGinnis, S. P.; Hochella, M. F., Jr.; Rejeski, D.; Hull, M. S. Nanotechnology in the real world: Redeveloping the nanomaterial consumer products inventory. *Beilstein J. Nanotechnol.* **2015**, *6*, 1769−1780.

(3) Nel, A.; Xia, T.; Mädler, L.; Li, N. Toxic potential of materials at the nanolevel. *Science* **2006**, *311*, 622−627.
(4) Murphy, C. J.; Vartanian, A. M.; Geiger, F. M.; Hamers, R. J.; Pedersen, J.; Cui, Q.; Haynes, C. L.; Carlson, E. E.; Hernandez, R.; Klaper, R. D.; Orr, G.; Rosenzweig, Z. Biological responses to engineered nanomaterials: Needs for the next decade. *ACS Cent. Sci.* **2015**, *1*, 117−123.
(5) Nie, L.; Nusantara, A. C.; Damle, V. G.; Baranov, M. V.; Chipaux, M.; Reyes-San-Martin, C.; Hamoh, T.; Epperla, C. P.; Guricova, M.; Cigler, P.; van den Bogaart, G.; Schirhagl, R. Quantum sensing of free radicals in primary human dendritic cells. *Nano Lett.* **2022**, *22*, 1818−1825.
(6) Mzyk, A.; Ong, Y.; Ortiz Moreno, A. R.; Padamati, S. K.; Zhang, Y.; Reyes-San-Martin, C. A.; Schirhagl, R. Diamond color centers in diamonds for chemical and biochemical analysis and visualization. *Anal. Chem.* **2022**, *94*, 225−249.
(7) Maurer-Jones, M. A.; Gunsolus, I. L.; Murphy, C. J.; Haynes, C. L. Toxicity of engineered nanoparticles in the environment. *Anal. Chem.* **2013**, *85*, 3036−3049.
(8) Dominguez, G. A.; Lohse, S. E.; Torelli, M. D.; Murphy, C. J.; Hamers, R. J.; Orr, G.; Klaper, R. D. Effects of charge and surface ligand properties of nanoparticles on oxidative stress and gene expression within the gut of Daphnia magna. *Aquat. Toxicol.* **2015**, *162*, 1−9.
(9) Allen, C.; Qiu, T. A.; Pramanik, S.; Buchman, J. T.; Krause, M. O. P.; Murphy, C. J. Research highlights: Investigating the role of nanoparticle surface charge in nano-bio interactions. *Environ. Sci.Nano* **2017**, *4*, 741−746.
(10) Buchman, J. T.; Hudson-Smith, N. V.; Landy, K. M.; Haynes, C. L. Understanding nanoparticle toxicity mechanisms to inform redesign strategies to reduce environmental impact. *Acc. Chem. Res.* **2019**, *52*, 1632−1642.
(11) Mensch, A. C.; Hernandez, R. T.; Kuether, J. E.; Torelli, M. D.; Feng, Z. V.; Hamers, R. J.; Pedersen, J. A. Natural organic matter concentration impacts the interaction of functionalized diamond nanoparticles with model and actual bacterial membranes. *Environ. Sci. Technol.* **2017**, *51*, 11075−11084.
(12) Mensch, A. C.; Melby, E. S.; Laudadio, E. D.; Foreman-Ortiz, I. U.; Zhang, Y.; Dohnalkova, A.; Hu, D.; Pedersen, J. A.; Hamers, R. J.; Orr, G. Preferential interactions of primary amine-terminated quantum dots with membrane domain boundaries and lipid rafts revealed with nanometer resolution. *Environ. Sci.Nano* **2020**, *7*, 149−161.
(13) Niemuth, N. J.; Williams, D. N.; Mensch, A. C.; Cui, Y.; Orr, G.; Rosenzweig, Z.; Klaper, R. D. Redesign of hydrophobic quantum dots mitigates ligand-dependent toxicity in the nematode. *C. elegans. Nanoimpact* **2021**, *22*, 100318.
(14) Zhang, Y.; Hudson-Smith, N. V.; Frand, S. D.; Cahill, M. S.; Davis, L. S.; Feng, Z. V.; Haynes, C. L.; Hamers, R. J. Influence of the spatial distribution of cationic functional groups at nanoparticle surfaces on bacterial viability and membrane interactions. *J. Am. Chem. Soc.* **2020**, *142*, 10814−10823.
(15) Gunsolus, I. L.; Haynes, C. L. Analytical aspects of nanotoxicology. *Anal. Chem.* **2016**, *88*, 451−479.
(16) Reineck, P.; Francis, A.; Orth, A.; Lau, D. W. M.; Nixon-Luke, R. D. V.; Das Rastogi, I.; Razali, W. A. W.; Cordina, N. M.; Parker, L. M.; Sreenivasan, V. K. A.; Brown, L. J.; Gibson, B. C. Brightness and photostability of emerging red and near-IR fluorescent nanomaterials for bioimaging. *Adv. Opt. Mater.* **2016**, *4*, 1549−1557.
(17) Stavis, C.; Clare, T. L.; Butler, J. E.; Radadia, A. D.; Carr, R.; Zeng, H.; King, W. P.; Carlisle, J. A.; Aksimentiev, A.; Bashir, R.; Hamers, R. J. Surface functionalization of thin-film diamond for highly stable and selective biological interfaces. *Proc. Natl. Acad. Sci. U.S.A.* **2011**, *108*, 983−988.
(18) Cordina, N. M.; Sayyadi, N.; Parker, L. M.; Everest-Dass, A.; Brown, L. J.; Packer, N. H. Reduced background autofluorescence for cell imaging using nanodiamonds and lanthanide chelates. *Sci. Rep.* **2018**, *8*, 4521.
(19) Chowdhury, S.; Chen, M.; Eckert, R.; Ren, D.; Wu, F.; Repina, N.; Waller, L. High-resolution 3d refractive index microscopy of multiple-scattering samples from intensity images. *Optica* **2019**, *6*, 1211−1219.
(20) Zhang, Y.; Tamijani, A. A.; Taylor, M. E.; Zhi, B.; Haynes, C. L.; Mason, S. E.; Hamers, R. J. Molecular surface functionalization of carbon materials via radical-induced grafting of terminal alkenes. *J. Am. Chem. Soc.* **2019**, *141*, 8277−8288.
(21) Yang, W.; Auciello, O.; Butler, J. E.; Cai, W.; Carlisle, J. A.; Gerbi, J. E.; Gruen, D. M.; Knickerbocker, T.; Lasseter, T. L.; Russell, J. N., Jr.; Smith, L. M.; Hamers, R. J. DNA-modified nanocrystalline diamond thin-films as stable, biologically active substrates. *Nat. Mater.* **2002**, *1*, 253−257.
(22) Hsiao, W. W.-W.; Hui, Y. Y.; Tsai, P.-C.; Chang, H.-C. Fluorescent nanodiamond: A versatile tool for long-term cell tracking, super-resolution imaging, and nanoscale temperature sensing. *Acc. Chem. Res.* **2016**, *49*, 400−407.
(23) Torelli, M. D.; Nunn, N. A.; Shenderova, O. A. A perspective on fluorescent nanodiamond bioimaging. *Small* **2019**, *15*, No. e1902151.
(24) Miller, B. S.; Bezinge, L.; Gliddon, H. D.; Huang, D.; Dold, G.; Gray, E. R.; Heaney, J.; Dobson, P. J.; Nastouli, E.; Morton, J. J. L.; McKendry, R. A. Spin-enhanced nanodiamond biosensing for ultrasensitive diagnostics. *Nature* **2020**, *587*, 588−593.
(25) Smith, B. R.; Inglis, D. W.; Sandnes, B.; Rabeau, J. R.; Zvyagin, A. V.; Gruber, D.; Noble, C. J.; Vogel, R.; Ōsawa, E.; Plakhotnik, T. Five-nanometer diamond with luminescent nitrogen-vacancy defect centers. *Small* **2009**, *5*, 1649−1653.
(26) Schirhagl, R.; Chang, K.; Loretz, M.; Degen, C. L. Nitrogen-vacancy centers in diamond: Nanoscale sensors for physics and biology. *Annu. Rev. Phys. Chem.* **2014**, *65*, 83−105.
(27) van der Laan, K.; Hasani, M.; Zheng, T.; Schirhagl, R. Nanodiamonds for in vivo applications. *Small* **2018**, *14*, No. e1703838.
(28) Yu, S.-J.; Kang, M.-W.; Chang, H.-C.; Chen, K.-M.; Yu, Y.-C. Bright fluorescent nanodiamonds: No photobleaching and low cytotoxicity. *J. Am. Chem. Soc.* **2005**, *127*, 17604−17605.
(29) Jones, Z. R.; Niemuth, N. J.; Robinson, M. E.; Shenderova, O. A.; Klaper, R. D.; Hamers, R. J. Selective imaging of diamond nanoparticles within complex matrices using magnetically induced fluorescence contrast. *Environ. Sci.Nano* **2020**, *7*, 525−534.
(30) Singam, S. K. R.; Motylewski, J.; Monaco, A.; Gjorgievska, E.; Bourgeois, E.; Nesladek, M.; Giugliano, M.; Goovaerts, E. Contrast induced by a static magnetic field for improved detection in nanodiamond fluorescence microscopy. *Phys. Rev. Appl.* **2016**, *6*, 064013.
(31) Torelli, M. D.; Nunn, N. A.; Jones, Z. R.; Vedelaar, T.; Padamati, S. K.; Schirhagl, R.; Hamers, R. J.; Shames, A. I.; Danilov, E. O.; Zaitsev, A.; Shenderova, O. A. High temperature treatment of diamond particles toward enhancement of their quantum properties. *Front. Phys.* **2020**, *8*, 205.
(32) Chapman, R.; Plakhoitnik, T. Background-free imaging of luminescent nanodiamonds using external magnetic field for contrast enhancement. *Opt. Lett.* **2013**, *38*, 1847−1849.
(33) Sarkar, S. K.; Bumb, A.; Wu, X.; Sochacki, K. A.; Kellman, P.; Brechbiel, M. W.; Neuman, K. C. Wide-field in vivo background free imaging by selective magnetic modulation of nanodiamond fluorescence. *Biomed. Opt. Express* **2014**, *5*, 1190−1202.
(34) Igarashi, R.; Yoshinari, Y.; Yokota, H.; Sugi, T.; Sugihara, F.; Ikeda, K.; Sumiya, H.; Tsuji, S.; Mori, I.; Tochio, H.; Harada, Y.; Shirakawa, M. Real-time background-free selective imaging of fluorescent nanodiamonds in vivo. *Nano Lett.* **2012**, *12*, 5726−5732.
(35) Robinson, M. E.; Ng, J. D.; Zhang, H.; Buchman, J. T.; Shenderova, O. A.; Haynes, C. L.; Ma, Z.; Goldsmith, R. H.; Hamers, R. J. Optically detected magnetic resonance for selective imaging of diamond nanoparticles. *Anal. Chem.* **2018**, *90*, 769−776.
(36) Fedotov, I. V.; Zheltikov, A. M. Background-free two-photon fluorescence readout via a three-photon charge-state modulation of nitrogen-vacancy centers in diamond. *Opt. Lett.* **2019**, *44*, 3737−3740.

https://doi.org/10.1021/acsmeasuresciau.2c00006
ACS Meas. Sci. Au 2022, 2, 351−360

(37) Wu, T.-J.; Tzeng, Y.-K.; Chang, W.-W.; Cheng, C.-A.; Kuo, Y.; Chien, C.-H.; Chang, H.-C.; Yu, J. Tracking the engraftment and regenerative capabilities of transplanted lung stem cells using fluorescent nanodiamonds. *Nat. Nanotechnol.* **2013**, *8*, 682−689.
(38) Claveau, S.; Kindermann, M.; Papine, A.; Díaz-Riascos, Z. V.; Délen, X.; Georges, P.; López-Alemany, R.; Tirado, Ò. M.; Bertrand, J.-R.; Abasolo, I.; Cigler, P.; Treussart, F. Harnessing subcellular-resolved organ distribution of cationic copolymer-functionalized fluorescent nanodiamonds for optimal delivery of active sirna to a xenografted tumor in mice. *Nanoscale* **2021**, *13*, 9280−9292.
(39) Corsi, A. K.; Wightman, B.; Chalfie, M. A transparent window into biology: A primer on Cenorhabditis elegans. *WormBook*; WormBook, 2015; Vol. *200*, pp 1−31.
(40) Schindelin, J.; Arganda-Carreras, I.; Frise, E.; Kaynig, V.; Longair, M.; Pietzsch, T.; Preibisch, S.; Rueden, C.; Saalfeld, S.; Schmid, B.; Tinevez, J.-Y.; White, D. J.; Hartenstein, V.; Eliceiri, K.; Tomancak, P.; Cardona, A. Fiji: An open-source platform for biological-image analysis. *Nat. Methods* **2012**, *9*, 676−682.
(41) Stiernagle, T. Maintenance of C. elegans. *WormBook*; WormBook, 2006; pp 1−11.
(42) Kim, S. T.; Saha, K.; Kim, C.; Rotello, V. M. The role of surface functionality in determining nanoparticle cytotoxicity. *Acc. Chem. Res.* **2013**, *46*, 681−691.
(43) Zhang, Y.; Dahal, U.; Feng, Z. V.; Rosenzweig, Z.; Cui, Q.; Hamers, R. J. Influence of surface ligand molecular structure on phospholipid membrane disruption by cationic nanoparticles. *Langmuir* **2021**, *37*, 7600−7610.
(44) Krueger, A.; Lang, D. Functionality is key: Recent progress in the surface modification of nanodiamond. *Adv. Funct. Mater.* **2012**, *22*, 890−906.
(45) Cui, S.; Hu, E. L. Increased negatively charged nitrogen-vacancy centers in fluorinated diamond. *Appl. Phys. Lett.* **2013**, *103*, 051603.
(46) Hauf, M. V.; Simon, P.; Aslam, N.; Pfender, M.; Neumann, P.; Pezzagna, S.; Meijer, J.; Wrachtrup, J.; Stutzmann, M.; Reinhard, F.; Garrido, J. A. Addressing single nitrogen-vacancy centers in diamond with transparent in-plane gate structures. *Nano Lett.* **2014**, *14*, 2359−2364.
(47) Petrakova, V.; Rehor, I.; Stursa, J.; Ledvina, M.; Nesladek, M.; Cigler, P. Charge-sensitive fluorescent nanosensors created from nanodiamonds. *Nanoscale* **2015**, *7*, 12307−12311.
(48) Petráková, V.; Taylor, A.; Kratochvílová, I.; Fendrych, F.; Vacík, J.; Kučka, J.; Štursa, J.; Cígler, P.; Ledvina, M.; Fišerová, A.; Kneppo, P.; Nesládek, M. Luminescence of nanodiamond driven by atomic functionalization: Towards novel detection principles. *Adv. Funct. Mater.* **2012**, *22*, 812−819.
(49) Rondin, L.; Dantelle, G.; Slablab, A.; Grosshans, F.; Treussart, F.; Bergonzo, P.; Perruchas, S.; Gacoin, T.; Chaigneau, M.; Chang, H.-C.; Jacques, V.; Roch, J.-F. Surface-induced charge state conversion of nitrogen-vacancy defects in nanodiamonds. *Phys. Rev. B: Condens. Matter Mater. Phys.* **2010**, *82*, 115449.

https://doi.org/10.1021/acsmeasuresciau.2c00006
ACS Meas. Sci. Au 2022, 2, 351−360